EUROfusion

WPBB-PR(18) 19962

D.V. Bachurin et al.

Ab initio study of Be and Be12Ti for fusion applications

Preprint of Paper to be submitted for publication in Intermetallics

This work has been carried out within the framework of the EUROfusion Consortium and has received funding from the Euratom research and training programme 2014-2018 under grant agreement No 633053. The views and opinions expressed herein do not necessarily reflect those of the European Commission.

Ab initio study of Be and $Be_{12}Ti$ for fusion applications

D.V. Bachurin, P.V. Vladimirov

February 2, 2018

Institute for Applied Materials – Applied Materials Physics, Karlsruhe Institute of Technology, 76344, Eggenstein-Leopoldshafen, Germany

Abstract

The paper applies ab initio methods for investigation of possible origin of the superior swelling resistance of titanium beryllide $Be_{12}Ti$ over beryllium. Both materials are considered as neutron multiplier materials in some design concepts of tritium breeding blanket of future fusion reactor. The only stable tetragonal crystal structure of $Be_{12}Ti$ was studied in this work. Hydrogen solution energy in all non-equivalent interstitial positions of $Be_{12}Ti$ was found to be lower than that for beryllium suggesting easier dissolution of hydrogen atoms in $Be_{12}Ti$. Maximal binding energy of hydrogen atoms in vacancy linearly decreases with the number of hydrogen atoms both in beryllium and $Be_{12}Ti$. Hydrogen binding in a vacancy is 0.4 eV lower in $Be_{12}Ti$, suggesting easier release of hydrogen from beryllide with respect to beryllium. No formation of chemical bounds between hydrogen atoms inside both beryllium and $Be_{12}Ti$ vacancies were observed.

Keywords: Ab initio calculations; Beryllium; Beryllides; Hydrogen; Vacancy

Corresponding author: D.V. Bachurin
E-mail address: dmitry.bachurin@kit.edu
Tel: +49 721 608-23639
Fax: +49 721 608-24567

1 Introduction

Intermetallic beryllium compounds possess number of outstanding properties which make them attractive for different industrial applications. Advanced mechanical properties such as high strength at elevated temperatures, excellent oxidation resistance and low density are indispensable for aerospace industry [1]. Be_2Ti compound demonstrates anomalous behavior in magnetic fields [2] and has a potential to be used as a hydrogen storage material [3].

Such compounds as $Be_{12}Ti$, $Be_{12}V$ and $Be_{12}Zr$ are considered as possible candidates for fusion applications, namely as neutron multiplier for breeder blanket of the demonstration nuclear fusion power reactor (DEMO) to be used instead of pure beryllium. Conceptual design of DEMO supposes an operation at significantly harder conditions in contrast to the International Thermonuclear Experimental Reactor ITER (stronger irradiation load and higher temperatures). Therefore such materials should obey high melting point, high oxidation resistance, low tritium retention and low swelling.

Materials working in fusion environment should withstand severe operation conditions including irradiation with fast neutrons. Collisions of the latter with atoms of material generate atomic displacement cascades in which individual point defects (vacancies and interstitials) and their clusters can be formed. Moreover, neutron induced transmutation results in accumulation of gaseous atoms (helium and hydrogen) which grately facilitate formation of gas bubbles and swelling at elevated temperatures [4–8].

Beryllides show higher resistance to volumetric swelling than pure beryllium. Usually, swelling of nuclear materials is associated with formation of gas bubbles promoted by helium. Vacancies in beryllium are also known to be efficient traps for hydrogen isotopes [9–11]. Gaseous atoms stabilize vacancy clusters allowing them to grow above the critical radius. Understanding of hydrogen trapping in irradiated beryllium and $Be_{12}Ti$ is extremely important for the reduction of tritium radioactive inventory within fusion reactor as well as for proper handling of radioactive wastes during decommissioning of the fusion blanket. On the other hand, facilitation of tritium release will significantly facilitate recycling of about 300 tons of beryllium pebbles required for the DEMO reactor blanket [12].

Among the plenty of experimental studies on beryllium compounds [13–21], there is a lack of theoretical understanding of the reason why beryllides demonstrate outstanding properties with respect to pure beryllium for fusion blanket applications.

The present paper is devoted to elucidation of the origin of accelerated tritium release from $Be_{12}Ti$ by performing comparison of hydrogen isotope retention properties with pure beryllium using ab initio methods. The paper is organized as follows. In section 3.1, we review recent situation with controversial interpretation of $Be_{12}Ti$ structure. Elastic moduli of Be and $Be_{12}Ti$ are calculated and compared with previous findings in section 3.2. Hydrogen solution energy in all non-equivalent interstitial positions of both Be and $Be_{12}Ti$ are calculated in section 3.3. Hydrogen binding energies with Be and $Be_{12}Ti$ vacancies are reported in section 3.4.

2 Computational methodology

Static ab initio calculations based on density functional theory were performed using simulation package VASP [22, 23]. The standard pseudopotentials for beryllium (with two valence electrons), titanium (with four valence electrons) and hydrogen were taken from the VASP library [24, 25]. The projector augmented wave potential (PAW) was used to describe the interactions between ions and electrons. The generalized gradient approximation (GGA) of Perdew and Wang [26] was employed to determine the exchange-correlation energy.

During static relaxations the volume and the shape of the simulation cell were fixed. No restrictions on relaxation of atoms within the cell were imposed. A Fermi broadening of 0.2 eV and the cut-off energy of the plane waves of 450 eV were chosen for both Be and $Be_{12}Ti$. The mesh of $15 \times 15 \times 15$ k-points was used for sampling of Brillouin zone. The cells of the sizes of $4 \times 4 \times 2$ (64 atoms) and $1 \times 1 \times 2$ (54 atoms) were used for computation of hydrogen solution as well as binding energies in Be and $Be_{12}Ti$, respectively. Periodic boundary conditions were applied along all crystalographic axes.

Atomic structures were visualized with the open source program Jmol [27].

3 Results and discussion

3.1 Structure and lattice parameters

3.1.1 Beryllium

Beryllium has a hexagonal close-packed (hcp) structure. The calculated lattice parameters for bulk beryllium [28–30] and comparison with some theoretical and

experimental data are presented in Table 1. More complete review of the studies devoted to determination of lattice constants is given in Refs. [31, 32].

3.1.2 Intermetallic $Be_{12}Ti$

Analysing the literature data on crystal structure of $Be_{12}Ti$ we faced with a controversial situation. Crystallographic databases (see e.g. ICSD [33]) report the structure of $Be_{12}Ti$ both as hexagonal $P6/mmm$ and tetragonal $I4/mmm$. Tracing back through the references we found that Raeuchle et. al. [34] were the first who determined the crystal structure of $Be_{12}Ti$ as disordered hexagonal with the space group of $P6/mmm$. Some years later, Raeuchle and von Batchelder [35] reported that the structure of $Be_{12}Mo$ is tetragonal with the space group of $I4/mmm$ and with the local atomic configuration similar to that of $Be_{12}Ti$. The molybdenum analogue was chosen since it was simpler for a study and belongs to the group of compounds obtaining the same crystal structure as $Be_{12}Ti$. Number of later publications [36–39] confirmed tetragonal structure $I4/mmm$ of $Be_{12}Ti$.

Recently Peng, Liu et al. [40, 41] have performed first-principle calculations of structural and elastic properties of $Be_{12}Ti$ with the use of the hexagonal structure erroneously identified by Raeuchle et al. in their first publication [34]. Our analysis have shown the non-equivalence of positional parameters of $Be_{12}Ti$ with tetragonal and hexagonal structures.

This controversy regarding the structure of $Be_{12}Ti$ were recently highlighted by Jackson et al [42], where detailed correspondence between the $I4/mmm$ tetragonal and the $P6/mmm$ hexagonal unit cell was considered. Namely, calculation of phonon dispersion curves has shown that the $P6/mmm$ hexagonal structures is unstable in the ground state (at the M-point). Such instability of the $P6/mmm$ structure should lead to hexagonal $\rightarrow$ tetragonal transformation and corresponding displacements of Ti and Be atoms. Liu et al. [41] have performed similar calculations and did not observed any instability at the M-point in the undeformed state, while imaginary phonon frequency was found at the A-point at high pressure of 45 GPa thus suggesting dynamical instability of hexagonal $Be_{12}Ti$ structure (see Fig. 5 in Ref. [41]).

We have repeated the calculation of formation energies of the tetragonal and hexagonal $Be_{12}Ti$ phases similar to that made by Jackson et el. [42] using the following expression

$$E_f = E_{total}^{\mathrm{Be_{12}Ti}} - n \cdot E^{\mathrm{Ti}} - m \cdot E^{\mathrm{Be}}, \qquad (1)$$

where $E_{total}^{\mathrm{Be_{12}Ti}}$ is the energy of the computational cell containing n titanium and m

beryllium atoms; E^{Ti}=−7.7432 eV and E^{Be}=−3.7278 eV are the cohesive energies per one titanium and one beryllium atoms, respectively. Calculation for the tetragonal and hexagonal $Be_{12}Ti$ phases gives −3.67 and 1.12 eV, respectively, suggesting that stability of the tetragonal phase and instability of the hexagonal one. A difference between formation energies of 4.79 eV is noticeably larger than that obtained in Ref. [42], i.e. 1.08 eV.

In the present work we use the tetragonal structure with the unit cell containing 24 beryllium and 2 titanium atoms as demonstrated in Fig. 1. For convenience, the Cartesian coordinates of all non-equivalent atoms within the tetragonal unit cell of $Be_{12}Ti$ are given in Table 4. The corresponding positional parameters for tetragonal cell are Be1(1/4,1/4,1/4), Be2(0.361,0,0), Be3(0.277,1/2,0) and Ti4(0,0,0). The optimized lattice parameters of $Be_{12}Ti$ at 0 K and zero external pressure are presented in table 1. As seen, our results are in a good agreement with experimentally measured values [37, 38]. Electron structure of $Be_{12}Ti$ was studied by Munakata et al. [43].

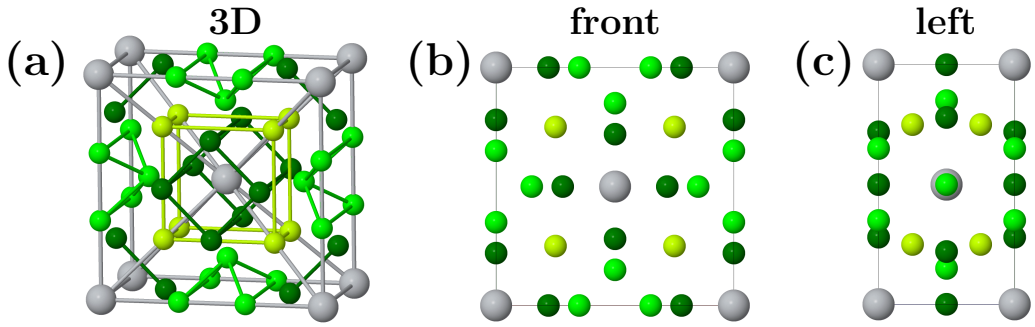

Figure 1: Crystallographic (tetragonal) structure of $Be_{12}Ti$: (a) three-dimensional, (b) the front and (c) the left views. Atoms are colored according to their type: Be1 (light green), Be2 (lime), Be3 (dark green) and Ti4 (grey).

3.2 Elastic properties

The elastic constants C_{ij} were calculated in the classical way via Taylor expansion of the total energy for the unit cell with respect to a small strain. Detailed descriptions of the strains and energy changes for hexagonal and tetragonal crystal structures can be found in Refs. [44–48]. Hexagonal beryllium crystal is characterized by five independent elastic constants: C_{11}, C_{12}, C_{13}, C_{33} and C_{44}, while tetragonal $Be_{12}Ti$ structure obtains all above listed moduli and C_{66}. For hexagonal structure the following relation is valid $C_{66} = (C_{11} - C_{12})/2$. Bulk modulus B and shear modulus

Table 1: The lattice constants a and c (Å) at 0 K for Be and $Be_{12}Ti$. The experimental values were measured at room temperature.

Material	a	c	c/a	Reference
Be	2.265	3.562	1.573	present work
Be	2.248	3.529	1.570	ab initio [58]
Be	2.286	3.584	1.568	experiment [59]
$Be_{12}Ti$	7.326	4.147	0.566	present work
$Be_{12}Ti$	7.359	4.164	0.566	ab initio [42]
$Be_{12}Ti$	7.350	4.190	0.570	experiment [37]
$Be_{12}Ti$	7.360	4.195	0.570	experiment [38]

Table 2: Elastic moduli C_{ij} (GPa) for beryllium and intermetallide $Be_{12}Ti$ calculated at 0 K. Corresponding values of the Young's modulus E, the bulk modulus B and the shear modulus G for polycrystalline aggregates are also presented.

Material	C_{11}	C_{12}	C_{13}	C_{33}	C_{44}	C_{66}	E	G	B
Be	344	14	-8	415	163	165	351	122	172
$Be_{12}Ti$	338	-8	58	240	125	79	280	126	124

G of a polycrystalline aggregate were determined from the calculated elastic constants C_{ij} using Voigt-Reuss-Hill approximation [45, 48–50]. The Young's modulus was then evaluated from the relation for isotropic materials $E = 9BG/(3B + G)$.

As seen in Fig. 2a, the calculated elastic moduli for beryllium are in general consistent with the previously published data [51–58]. However, the magnitude of the moduli C_{11}, C_{33}, C_{66}, E and B are somewhat higher. Negative value for C_{13} was obtained in our simulations (see Table 2), which is also confirmed experimentally [52]. The measurements [51] have shown that C_{12} might be also negative. In beryllium C_{12} is positive, but much lower in comparison with the other elastic moduli.

Figure 2b demonstrates the elastic constants for $Be_{12}Ti$ compound. The module C_{12} is found to be negative. We are aware of the only one publication, where the stiffness constants C_{ij} obtained via density functional theory were reported for tetragonal structure of $Be_{12}Ti$ [42]. The values of C_{11} and C_{33} are higher, C_{13} is lower, while all other moduli differ insignificantly as compared to our data. For comparison

Fig. 2b shows also the results of Peng [40], which obviously are not consistent with our findings due to different crystal structure of $Be_{12}Ti$ used in their work. Experimental values measured at 20°C for $Be_{12}Ti$ are: 282 GPa for the Young's modulus, 128 GPa for shear modulus and 117 GPa for the bulk modulus [60]. These are in a very good agreement with our values obtained using Voigt-Reuss-Hill approach (see Fig. 2b).

All calculated elastic constants C_{ij} fulfil the mechanical stability criteria for hexagonal (Be) and tetragonal ($Be_{12}Ti$) systems [61, 62]: $C_{11} > |C_{12}|$, $C_{33}(C_{11} + C_{12}) > 2C_{13}^2$, $C_{44} > 0$ and $C_{66} > 0$. The anisotropy factor $A = 2C_{44}/(C_{11} - C_{12})$ is equal to 0.99 for Be and 0.72 for $Be_{12}Ti$. This large deviation from the unity illustrates the strong anisotropy of intermetallic $Be_{12}Ti$. For comparison, we have calculated also the elastic constants for the unstable hexagonal phase of $Be_{12}Ti$. Surprisingly, they also fulfil the mechanical stability criteria suggesting that the latter is necessary, but not sufficient condition.

3.3 Hydrogen in interstitial position

Evaluation of hydrogen retention behavior is very important especially from the point of view of assessment of tritium radioactive inventory in pebbles for handling of the radioactive waste after the end-of-life of the blanket. Such characteristic as solution energy is responsible for dissolution of hydrogen atoms. The solution energy was defined as

$$E_s = E_{total}^{\mathrm{X+H}} - E_{total}^{\mathrm{X}} - \frac{1}{2} \cdot E_{ref}^{\mathrm{H_2}}, \tag{2}$$

where $E_{total}^{\mathrm{X+H}}$ and E_{total}^{X} (X=Be, $Be_{12}Ti$) are the energies of simulation cell with and without hydrogen; $1/2 \cdot E_{ref}^{\mathrm{H_2}} = -3.3590$ eV is the energy of one hydrogen atom in H_2 molecule. Diffusion of hydrogen atoms in metal lattices occurs by jumping from one interstitial site into another. Further hydrogen solution energies in all non-equivalent interstitial sites were calculated for both beryllium and $Be_{12}Ti$ compound.

3.3.1 Beryllium

There are four non-equivalent high-symmetry interstitials positions for hydrogen in hexagonal lattice of beryllium. Two of them, tetrahedral and octahedral, are located between the neighboring basal planes, while basal tetrahedral and basal octahedral are projections of tetrahedral and octahedral positions onto basal plane. However, as shown by Ganchenkova et al. [63], only two of them (basal tetrahedral

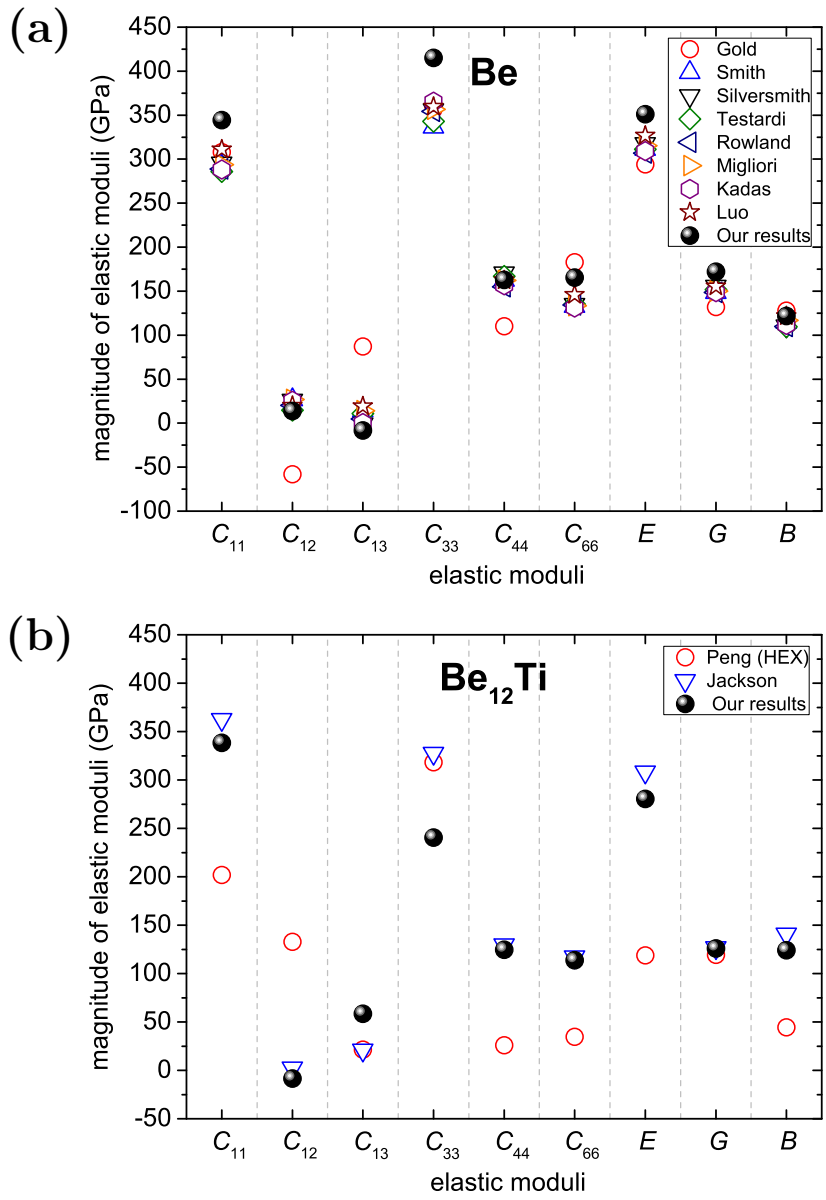

Figure 2: Comparison of elastic moduli C_{ij} (GPa) for beryllium (a) and intermetallic $Be_{12}Ti$ (b) at 0 K with the previously reported theoretical and experimental data. The bulk modulus B and shear modulus G were calculated using the Voigt-Reuss-Hill approach. The Young's modulus E was determined with the help of the classical relation for isotropic materials.

and octahedral) are found to be stable. Figure 3 illustrates these positions in hexagonal lattice of beryllium. The energies of hydrogen located at basal tetrahedral and octahedral interstitial positions are 1.54 and 1.74 eV, respectively. Obtained results are very close to those found in Refs. [63, 64].

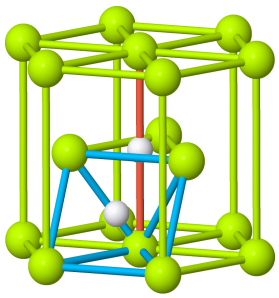

Figure 3: Stable interstitials positions of hydrogen (white) in hexagonal lattice of beryllium (green). Red lines connect hydrogen atom at basal tetrahedral site with adjucent beryllium atoms above and below it. Half of the octahedral hole containing hydrogen atom is drawn with blue lines.

3.3.2 Intermetallic $Be_{12}Ti$

Tetragonal lattice of $Be_{12}Ti$ contains four crystallographcally non-equivalent positions: three occupied with beryllium (denoted as Be1, Be2 and Be3) and one with titanium (denoted as Ti4) as demonstrated in Fig. 1. The first shell atomic environment for these atoms are presented in Fig. 4.

Initially every hydrogen interstitial position was chosen to be equidistant from all the vertices of a tetrahedron formed by four neighboring atoms within the lattice of $Be_{12}Ti$. The results of calculation of solution energy for hydrogen atom in all non-equivalent interstitial positions are summarized in Table 3 and plotted in Fig. 5. As seen, hydrogen solution energy is completely determined by the local environment of hydrogen atom and is varied within the range from 0.43 to 1.38 eV. Note, that the corresponding value of the solution energy at the most favorable stable interstitial site (basal tetrahedral) in beryllium is 1.54 eV, which is at least 0.2 eV higher. The latter fact clearly suggests that dissolution of hydrogen atoms in $Be_{12}Ti$ should occur easier in comparison with beryllium.

Recently similar calculations of hydrogen solution energy at six interstitial sites in the lattice of $Be_{12}Ti$ were performed by Fujii et al [65]. They also found that the solution energies are positive for all studied configurations and change from 0.11 to

1.06 eV, i.e. in the range of 0.95 eV, which is in accordance with our findings. It seems that there is a systematic shift between the solution energies from [65] and ours, which might be tentatively explained by the difference in the reference energies used for hydrogen molecule in formula (2).

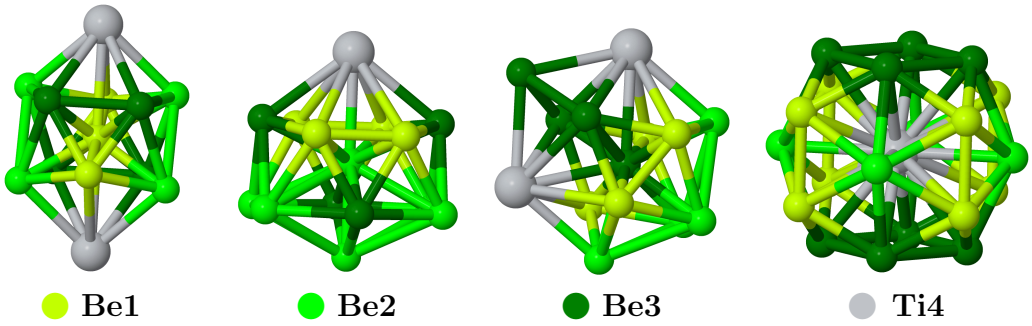

Figure 4: The first shell atomic environment for four non-equivalent positions in tetragonal crystal lattice of $Be_{12}Ti$. Atoms are colored accordingly: Be1 (light green), Be2 (lime), Be3 (dark green) and Ti4 (grey). Before relaxation hydrogen atoms were placed in all possible tetrahedrons formed by four non-equivalent neighboring atoms.

3.4 Hydrogen in monovacancy

Such characteristics as hydrogen binding energy reflects the ability of hydrogen atoms to be trapped by a vacancy. The binding energy of hydrogen with monovacancy in beryllium and $Be_{12}Ti$ was calculated using the following expression:

$$E_b = E_V^{(n-1)H} + E_{int}^H - E_V^{nH} - E_{bulk} \tag{3}$$

where $E_V^{(n-1)H}$ and E_V^{nH} are the total energies of the system containing $(n-1)$ and n hydrogen atoms, respectively; E_{int}^H is the most favorable energy among the configurations containing one hydrogen atom at interstitial site; E_{bulk} is the energy of the ideal lattice. As follows from the expression (3), negative energy means an absence of binding.

Monovacancy was chosen since the formation of divacancies in beryllium is energetically unfavorable irrespective of the divacancy orientation [66]. Similar results were obtained recently by Jackson et al. [67] for $Be_{12}Ti$ who showed that divacancies are also unstable with the only exception of Be2-Be2 divacancy with the binding energy close to zero.

Table 3: Non-equivalent interstitial positions for hydrogen in tetragonal lattice of $Be_{12}Ti$. For brevity, beryllium atoms Be1, Be2 and Be3 are denoted by numbers 1, 2 and 3, titanium atom Ti4 as 4. Each tetrahedron is represented by a sequence of four digits designating type of the atoms located at its vertices, i.e. i-j-k-l, where i, j, k, l=1,4. $E_s^{\mathrm{Be1-3/Ti4}}$ in eV is the solution energy for one hydrogen atom calculated using expression (2).

Be**1**	E_s^{Be1}	Be**2**	E_s^{Be2}	Be**3**	E_s^{Be3}	Ti**4**	E_s^{Ti4}
1-1-2-3	1.18	1-1-**2**-3	1.18	1-1-2-**3**	1.18	1-1-2-**4**	0.82
1-1-2-4	0.82	1-1-**2**-4	0.82	1-1-**3**-3	1.38	1-2-3-**4**	0.66
1-1-3-3	1.30	1-**2**-2-3	1.01	1-2-2-**3**	1.01	1-3-3-**4**	0.76
1-2-2-3	1.01	1-**2**-3-4	0.66	1-2-**3**-4	0.66	3-3-3-3	0.43
1-2-3-4	0.66	**2**-2-2-2	0.90	1-**3**-3-4	0.76		
1-3-3-4	0.76	**2**-2-2-3	0.85	2-2-2-**3**	0.85		
				3-3-3-4	0.43		

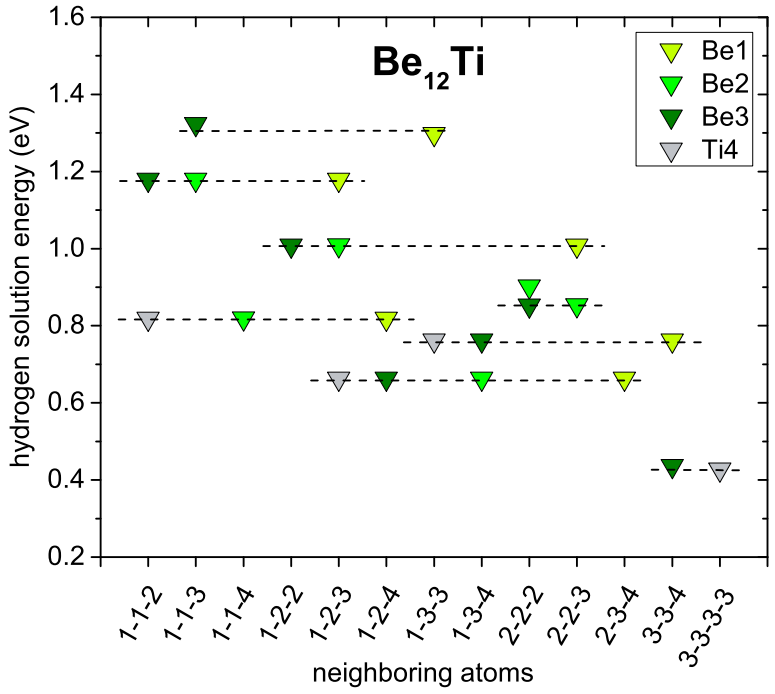

Figure 5: Solution energy for all non-equivalent hydrogen interstitial positions in tetragonal crystal lattice of $Be_{12}Ti$. Horizontal dashed lines connect position with the same local environment. Notation of tetrahedra is explaned in the caption to Table 3.

3.4.1 Beryllium

Our simulations demonstrate that single hydrogen atom is unstable in the center of beryllium vacancy. Addition of two and more hydrogen atoms does not lead to a formation of chemically bound hydrogen molecule, which is also consistent with the earlier predictions [63, 68]. Single vacancy in beryllium can accommodate up to five hydrogen atoms [63]. The binding energy as a function of the number of hydrogen atoms in vacancy $E_b^{VH}(n)$ is displayed in Fig. 6. As seen, $E_b^{VH}(n)$ decreases with increase of n and can be fitted with the following linear function:

$$E_b^{VH}(n) = 1.2 - 0.2(n-1). \tag{4}$$

The binding energy for single hydrogen atom in a vacancy in BT position is 1.21 eV. The trap of second, third etc. hydrogen atoms noticeably reduces the binding energy. For instance, $E_b^{VH}(5)$ is of about 0.4 eV (see Fig. 6). Thus, the higher is the amount of hydrogen atoms, the weaker they are bound within beryllium vacancy. Data in Fig. 6 are systematically lower by an average of 0.1 eV as compared with those reported in Ref. [63], which is related to the usage of different pseudopotential. In addition, the difference between the binding energies of hydrogen in 2T2 (T2 stands for tetrahedral position slightly shifted upwards with respect to normal tetrahedral position T) and BT+T2 (BT stands for basal tetrahedral position) configurations is noticeably smaller than obtained by Ganchenkova et al [63].

3.4.2 Intermetallic $Be_{12}Ti$

The binding energy of hydrogen-vacancy complex was calculated for all four types of monovacancies corresponding to the absence of each non-equivalent atoms in the unit cell of $Be_{12}Ti$. In order to avoid running through all possible combinations of first and subsequent hydrogen atoms within a vacancy, the following procedure for their arrangement was applied. (1) The first hydrogen atom was positioned within triangle faces formed by the first coordination shell of a vacancy. Non-equivalent hydrogen sites were denoted in the same way as interstitial positions in the section 3.3 but using three digits designating apexes of the triangle face, i.e. *i*-*j*-*k*, where i, j, k=1,3. Unique identification of each hydrogen position within vacancy is ensured by addition of the fourth index corresponding to the type of the removed atom (Be1, Be2, Be3 or Ti4) which index is typed in boldface. (2) The configuration with the highest binding energy was chosen from the results obtained on previous step and the next hydrogen atom was positioned at all non-equivalent empty sites. (3) This

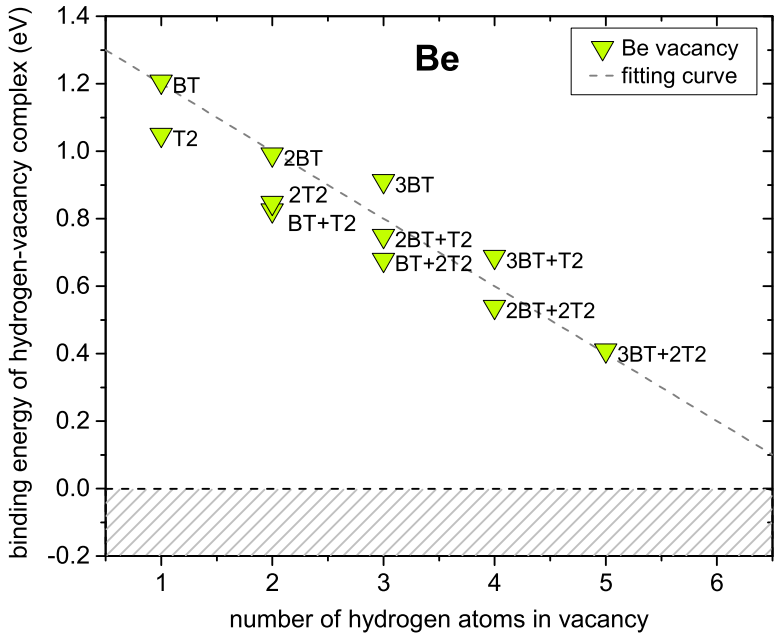

Figure 6: Binding energy of hydrogen-vacancy complex in beryllium for different number of hydrogen atoms in a vacancy. Shaded area illustrates the region with negative binding energy. Dashed line is an approximate linear fit through the data.

procedure was repeated for subsequent hydrogen atom placing.

The results of calculations for one hydrogen atom are presented in Fig. 7a. The binding energies strongly depend on the specific hydrogen position and vary in the range from -0.2 to 0.8 eV. For instance, hydrogen has no binding at 2-2-3 site within Be1 vacancy, while maximal binding energy appears to be at 1-3-4 site within Be2 vacancy. It is interesting to note that the values of the binding energy of hydrogen with vacancy in beryllium are higher by at least 0.25 and 0.4 eV (for T2 and BT sites, respectively) than the maximal value of the binding energy of hydrogen with vacancies in $Be_{12}Ti$.

Dependence of the binding energy for two, three and four hydrogen atoms in all types of vacancies are demonstrated in Fig. 7b. In order to avoid an overlapping, the dots corresponding to the same number of hydrogen atoms were slightly displaced along the abscissa. Figure 7b shows a clear decrease of maximal binding energy with the increase of the number of hydrogen atoms similar to that found in beryllium (see Fig. 6). The binding energy significantly depends on hydrogen adsorption site. For every number of hydrogen atoms within vacancy, there are sites at which hydrogen has no binding. All other binding energies for a certain number of hydrogen atoms

are more or less uniformly distributed between their maximum and minimum values. Vacancies with more than four hydrogen atoms were not studied in the present work. Hydrogen atoms in a vacancy are often three-coordinated with metal atoms and rarely are two-coordinated with the length of bond between 1.40 and 1.67Å. The distances between hydrogen atoms in all types of vacancies are in the range of 1.6−2.7Å, i.e. much larger than the bond length of the H_2 molecule.

Similar to the case of pure beryllium the maximum values of $E_b^{VH}(n)$ can be fitted as:

$$E_b(n) = 0.8 - 0.2(n-1). \tag{5}$$

Using Eq. (5) one can estimate that for five hydrogen atoms inside a vacancy the binding energy close to zero is expected.

For all investigated vacancy types with hydrogen occupation up to four atoms in $Be_{12}Ti$ and five in beryllium, no formation of hydrogen molecule was observed. Analysis of electron density maps confirms an absence of chemical bond between hydrogen atoms. In addition, our simulations demonstrate that hydrogen atoms prefer to occupy the periphery of vacancy similar to that found previously for beryllium [63] and other metals [69–73]

As follows from the obtained results, single hydrogen atom is weaker bound in $Be_{12}Ti$ (0.8 eV) than in pure beryllium (1.3 eV). According to the extrapolation of the obtained binding energies, less than seven hydrogen atoms can be bound in a beryllium vacancy, whereas only four in $Be_{12}Ti$. If the same tendency will be confirmed for trapping of helium, the lower swelling of beryllides might be traced back to the lower trapping ability of gaseous atoms within a vacancy.

4 Conclusions

The origin of the superior properties of titanium beryllide $Be_{12}Ti$ over beryllium by comparison of the corresponding properties of both materials were studied using ab initio methods. The main conclusions can be summarized as follows.

1. Structure and lattice parameters for beryllium and $Be_{12}Ti$ with tetragonal lattice structure were calculated. Elastic constants for both the materials are consistent with the available experimental and theoretical studies.

2. Hydrogen solution energy in interstitial positions of $Be_{12}Ti$ are at least 0.2 eV lower then that for beryllium suggesting easier dissolution of hydrogen atoms in $Be_{12}Ti$.

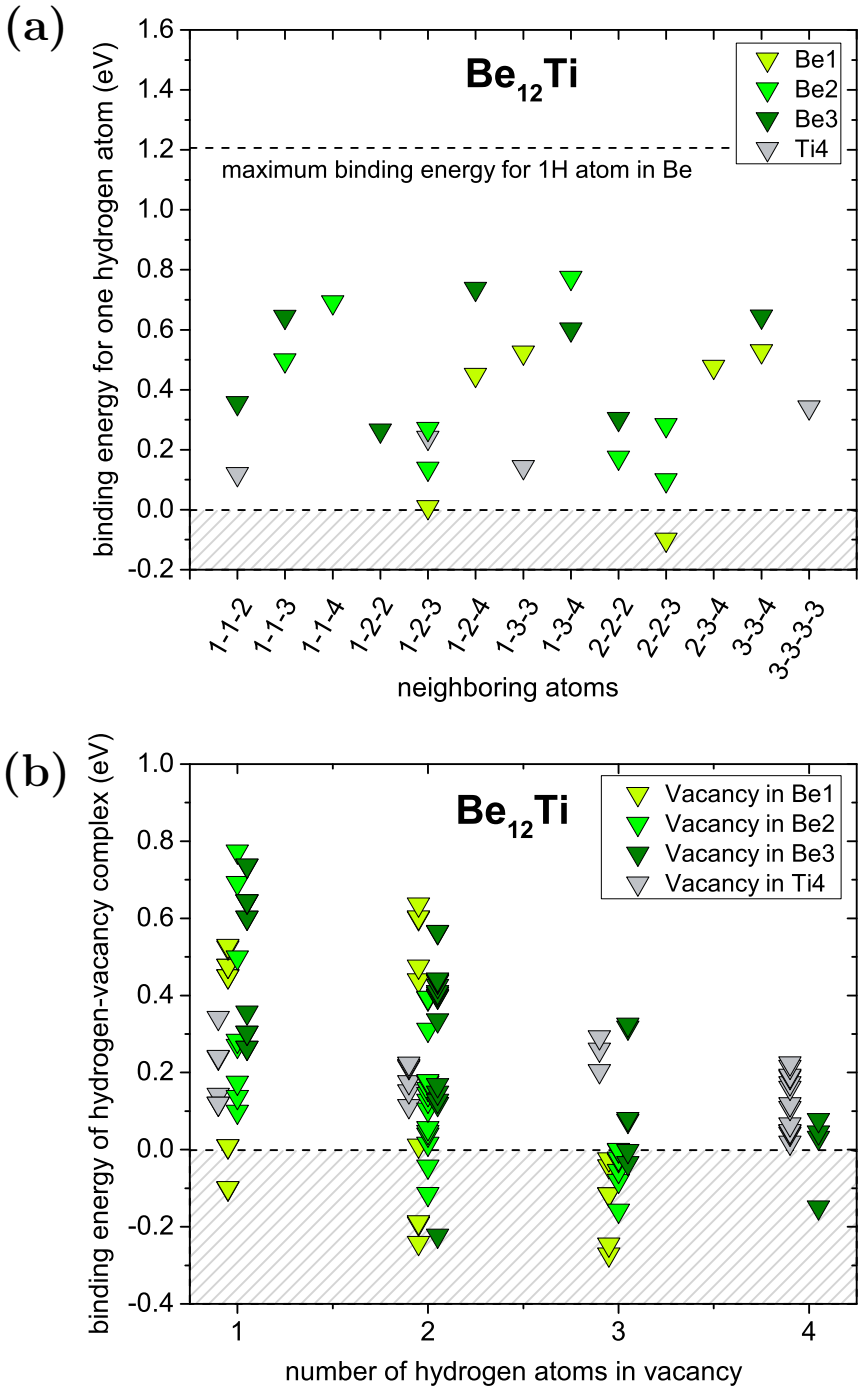

Figure 7: Binding energy of (a) one hydrogen atom located at all non-equivalent sites within four types of vacancies in $Be_{12}Ti$ and (b) hydrogen-vacancy complex in $Be_{12}Ti$ for different number of hydrogen atoms in a vacancy. Shaded area illustrates the region with negative binding energy. Horizontal dashed line in (a) demonstrates maximum binding energy of one hydrogen atom in beryllium monovacancy [63].

3. Maximal binding energy of hydrogen atoms in a vacancy decreases linearly with the number of hydrogen atoms both in beryllium and $Be_{12}Ti$. Hydrogen binding in vacancy is 0.4 eV lower in $Be_{12}Ti$, suggesting lower trapping ability of hydrogen from beryllide with respect to beryllium. This fact explains earlier hydrogen release during thermal desorption experiments (i.e. at lower temperatures) from $Be_{12}Ti$.

4. No formation of chemical bounds between hydrogen atoms inside both beryllium and $Be_{12}Ti$ vacancies were observed up to five hydrogen atoms in Be and four in $Be_{12}Ti$.

Acknowledgements

This work has been carried out within the framework of the EUROfusion Consortium and has received funding from the Euratom research and training programme 2014-2018 under grant agreement No 633053. The views and opinions expressed herein do not necessarily reflect those of the European Commission. Computational resources were provided by the IFERC Computational Simulation Centre (Rokkasho, Japan) and the Steinbuch Centre for Computing (Karlsruhe, Germany). The authors acknowledge support by the state of Baden-Wrttemberg through bwHPC and the German Research Foundation (DFG) through grant no INST 40/467-1 FUGG.

Appendix A. Cartesian coordinates of atoms in tetragonal unit cell of $Be_{12}Ti$

Table 4: The Cartesian coordinates (in Å) of all non-equivalent atoms within the tetragonal unit cell of $Be_{12}Ti$ with the lattice parameters $a = 7.326$Å and $c = 4.147$Å.

Number	Atom	Atom Type	x	y	z
1	Be	1	1.831	1.831	1.037
2	Be	2	2.572	7.326	4.147
3	Be	3	2.069	3.663	4.147
4	Be	1	5.494	5.494	3.111
5	Be	2	4.754	7.326	4.147
6	Be	3	5.257	3.663	4.147
7	Be	1	5.494	1.831	1.037
8	Be	1	5.494	5.494	1.037
9	Be	1	1.831	5.494	1.037
10	Be	2	7.326	2.572	4.147
11	Be	2	7.326	4.754	4.147
12	Be	3	3.663	2.069	4.147
13	Be	3	3.663	5.257	4.147
14	Be	3	1.831	5.494	3.111
15	Be	1	1.831	1.831	3.111
16	Be	1	5.494	1.831	3.111
17	Be	1	6.235	3.663	2.074
18	Be	2	3.663	6.235	2.074
19	Be	2	1.091	3.663	2.074
20	Be	2	3.663	1.091	2.074
21	Be	2	5.732	7.326	2.074
22	Be	3	7.326	5.732	2.074
23	Be	3	1.594	7.326	2.074
24	Be	3	7.326	1.594	2.074
25	Ti	4	7.326	7.326	4.147
26	Ti	4	3.663	3.663	2.074

References

[1] S.M. Bruemmer, B.W. Arey, J.L. Brimhall, J.P. Hirth. Hot-Hardness Comparisons among Isostructural Be12X Intermetallic Compounds, J Mater Res 8 (1993) 1550-1557.

[2] H. Yamada, K. Terao. High-field magnetism of TiBe2, Physica B 246 (1998) 502-504.

[3] B.C. Hauback, H. Fjellvag, A.J. Maeland. Temperature-Induced Structural-Changes in Be2ZrD15 Studied by Powder Neutron-Diffraction, J Alloy Compd 224 (1995) 241-243.

[4] J.B. Condon, T. Schober. Hydrogen Bubbles in Metals, J Nucl Mater 207 (1993) 1-24.

[5] P.B. Johnson, D.J. Mazey. Helium Gas Bubble Lattices in Face-Centerd-Cubic Metals, Nature 276 (1978) 595-596.

[6] P.B. Johnson, D.J. Mazey. Gas-Bubble Superlattice Formation in Bcc Metals, J Nucl Mater 218 (1995) 273-288.

[7] F.E. Lawson, P.B. Johnson. A temperature threshold for gas-bubble superlattice formation in molybdenum, J Nucl Mater 252 (1998) 34-42.

[8] V.P. Chakin, Z.Y. Ostrovsky. Evolution of beryllium microstructure under high-dose neutron irradiation, J Nucl Mater 307 (2002) 657-663.

[9] M. Reinelt, C. Linsmeier. Temperature programmed desorption of 1 keV deuterium implanted into clean beryllium, Phys Scripta T128 (2007) 111-114.

[10] V. Chakin, R. Rolli, A. Moeslang, M. Klimenkov, M. Kolb, P. Vladimirov, P. Kurinskiy, H.C. Schneider, S. van Til, A.J. Magielsen, M. Zmitko. Tritium release and retention properties of highly neutron-irradiated beryllium pebbles from HIDOBE-01 experiment, J Nucl Mater 442 (2013) S483-S489.

[11] V.N. Chernikov, V.K. Alimov, A.V. Markin, A.E. Gorodetsky, S.L. Kanashenko, A.P. Zakharov, I.B. Kupriyanov. Gas-induced swelling of beryllium implanted with deuterium ions, J Nucl Mater 233 (1996) 860-864.

[12] F. Hernandez, P. Pereslavtsev, Q. Kang, P. Norajitra, B. Kiss, G. Nadasi, O. Bitz. A new HCPB breeding blanket for the EU DEMO: Evolution, rationale and preliminary performances, Fusion Eng Des 124 (2017) 882-886.

[13] V. Chakin, M. Klimenkov, R. Rolli, P. Kurinskiy, A. Moeslang, C. Dorn. Microstructural and tritium release examination of titanium beryllides, J Nucl Mater 417 (2011) 769-774.

[14] P. Kurinskiy, V. Chakin, A. Moeslang, R. Rolli, E. Alves, L.C. Alves, N. Franco, C. Dorn, A.A. Goraieb. Comparative study of fusion relevant properties of Be12V and Be12Ti, Fusion Eng Des 86 (2011) 2454-2457.

[15] P. Kurinskiy, A. Moeslang, V. Chakin, M. Klimenkov, R. Rolli, S. van Til, A.A. Goraieb. Characteristics of microstructure, swelling and mechanical behaviour of titanium beryllide samples after high-dose neutron irradiation at 740 and 873 K, Fusion Eng Des 88 (2013) 2198-2201.

[16] P. Kurinskiy, R. Rolli, J.H. Kim, M. Nakamichi. Mechanical behavior of Be-Ti pebbles at blanket relevant temperatures, Fusion Eng Des 109 (2016) 764-767.

[17] J.H. Kim, M. Nakamichi. Effect of grain size on the hardness and reactivity of plasma-sintered beryllium, J Nucl Mater 453 (2014) 22-26.

[18] J.H. Kim, H. Iwakiri, T. Furugen, M. Nakamichi. Synthesis and reactivity of single-phase Be17Ti2 intermetallic compounds, Fusion Eng Des 102 (2016) 44-49.

[19] J.H. Kim, M. Nakamichi. Synthesis and characteristics of ternary Be-Ti-V beryllide pebbles as advanced neutron multipliers, Fusion Eng Des 109 (2016) 1764-1768.

[20] M. Nakamichi, J.H. Kim, K. Ochiai. Beryllide pebble fabrication of Be-Zr compositions as advanced neutron multipliers, Fusion Eng Des 109 (2016) 1719-1723.

[21] J.H. Kim, M. Miyamoto, Y. Hujii, M. Nakamichi, Reactivity and deuterium retention properties of titanium-beryllium intermetallic compounds, Intermetallics 82 (2017) 20-25.

[22] G. Kresse, J. Hafner. Ab initio Molecular-Dynamics for Liquid-Metals, Phys Rev B 47 (1993) 558-561.

[23] G. Kresse, J. Furthmuller. Efficient iterative schemes for ab initio total-energy calculations using a plane-wave basis set, Phys Rev B 54 (1996) 11169-11186.

[24] P.E. Blöchl. Projector Augmented-Wave Method, Phys Rev B 50 (1994) 17953-17979.

[25] G. Kresse, D. Joubert. From ultrasoft pseudopotentials to the projector augmented-wave method, Phys Rev B 59 (1999) 1758-1775.

[26] J.P. Perdew, Y. Wang. Accurate and Simple Analytic Representation of the Electron-Gas Correlation-Energy, Phys Rev B 45 (1992) 13244-13249.

[27] Jmol: an open-source Java viewer for chemical structures in 3D. http://www.jmol.org/

[28] D.V. Bachurin, P.V. Vladimirov. Ab initio study of hydrogen on beryllium surfaces, Surf Sci 641 (2015) 198-203.

[29] D.V. Bachurin, P.V. Vladimirov. Simulation of hydrogen effect on equilibrium shape of gas bubbles in beryllium, Fusion Eng Des 109 (2016) 1432-1436.

[30] D.V. Bachurin, P.V. Vladimirov. Ab initio study of beryllium surfaces with different hydrogen coverages, Acta Mat 134 (2017) 81-92.

[31] E. Wachowicz, A. Kiejna, J Phys: Condens Matter 13 (2001) 10767-10776.

[32] A. Allouche, M. Oberkofler, M. Reinelt, C. Linsmeier, Quantum Modeling of Hydrogen Retention in Beryllium Bulk and Vacancies. J Phys Chem C 114 (2010) 3588-3598.

[33] Inorganic Crystal Structure Database. https://icsd.fiz-karlsruhe.de/search/basic.xhtml

[34] R.F. Raeuchle, R.E. Rundle, The structure of $TiBe_{12}$. Acta Crystallogr 5 (1952) 85-93.

[35] R.F. Raeuchle, F. W. von Batchelder, The structure of $MoBe_{12}$. Acta Crystallogr 8 (1955) 691-694.

[36] J.V. Florio, R.E. Rundle, A.I. Snow, Acta Crystallogr 5 (1952) 449-457.

[37] A. Zalkin, D.E. Sands, O.H. Krikorian, R.G. Bedford, Beryllides of Ti, V, Cr, Zr, Nb, Mo, Hf, and Ta. Acta Crystallogr 14 (1961) 63-65.

[38] E. Gillam, H.P. Rooksby, Structural relationships in beryllium-titanium alloys. Acta Crystallogr 17 (1964) 762-763.

[39] D.M. Collins, M.C. Mahar, Acta Crystallogr C40 (1984) 914-915.

[40] S.M. Peng, Theoretical investigations on the structural, elastic and electronic properties of binary Beryllides under pressure. J Nucl Mater 464 (2015) 230-235.

[41] X.K. Liu, W. Zhou, X. Liu, S.M. Peng, First-principles investigation of the structural and elastic properties of $Be_{12}Ti$ under high pressure. RSC Adv 5 (2015) 59648-59654.

[42] M.L. Jackson, P.A. Burr, R.W. Grimes, Resolving the structure of $TiBe_{12}$. Acta Crystallogr B 72 (2016) 277-280.

[43] K. Munakata, H. Kawamura, M. Uchida, Kinetics of reaction with water vapor and ab initio study of titanium beryllide. J Nucl Mater 367 (2007) 1057-1062.

[44] L. Fast, J.M. Wills, B. Johansson, O. Eriksson, Elastic-Constants of Hexagonal Transition-Metals - Theory. Phys Rev B 51 (1995) 17431-17438.

[45] I.R. Shein, V.S. Kiiko, Y.N. Makurin, M.A. Gorbunova, A.L. Ivanovskii, Elastic parameters of single-crystal and polycrystalline wurtzite-like oxides BeO and ZnO: Ab initio calculations. Phys Solid State 49 (2007) 1067-1073.

[46] K.Y. Chen, K.P. Boyle, Elastic Properties, Thermal Expansion Coefficients, and Electronic Structures of Mg and Mg-Based Alloys. Metall Mater Trans A 40A (2009) 2751-2760.

[47] M.J. Mehl, J.E. Osburn, D.A. Papaconstantopoulos, B.M. Klein, Structural-Properties of Ordered High-Melting-Temperature Intermetallic Alloys from 1st-Principles Total-Energy Calculations. Phys Rev B 41 (1990) 10311-10323.

[48] T. Ouahrani, A. Otero-de-la-Roza, A.H. Reshak, R. Khenata, H.I. Faraoun, B. Amrani, M. Mebrouki, V. Luana, Elastic properties and bonding of the AgGaSe2 chalcopyrite. Physica B 405 (2010) 3658-3664.

[49] H.C. Zhai, X.F. Li, J.Y. Du, First-Principles Calculations on Elasticity and Anisotropy of Tetragonal Tungsten Dinitride under Pressure. Mater Trans 53 (2012) 1247-1251.

[50] R. Hill, The Elastic Behaviour of a Crystalline Aggregate. P Phys Soc Lond B 65 (1952) 349-354.

[51] L. Gold, Evaluation of the Stiffness Coefficients for Beryllium from Ultrasonic Measurements in Polycrystalline and Single Crystal Specimens. Phys Rev 77 (1950) 390-395.

[52] D.J. Silversmith, B.L. Averbach, Pressure Dependence of Elastic Constants of Beryllium and Beryllium-Copper Alloys. Phys Rev B 1 (1970) 567-571.

[53] J.F. Smith, C.L. Arbogast, Elastic Constants of Single Crystal Beryllium. J Appl Phys 31 (1960) 99-102.

[54] L.R. Testardi, J.H. Condon, Landau Quantum Oscillations of Velocity of Sound in Beryllium - Strain Dependence of Fermi Surface. Phys Rev B 1 (1970) 3928-3942.

[55] W.D. Rowland, J.S. White, The determination of the elastic constants of beryllium in the temperature range 25 to 300°C. J Phys F: Metal Phys 2 (1972) 231-236.

[56] A. Migliori, H. Ledbetter, D.J. Thoma, T.W. Darling, Beryllium's monocrystal and polycrystal elastic constants. J Appl Phys 95 (2004) 2436-2440.

[57] K. Kadas, L. Vitos, R. Ahuja, B. Johansson, J. Kollar, Temperature-dependent elastic properties of alpha-beryllium from first principles. Phys Rev B 76 (2007) 235109.

[58] F. Luo, L.C. Cai, X.R. Chen, F.Q. Jing, D. Alfe, Ab initio calculation of lattice dynamics and thermodynamic properties of beryllium. J Appl Phys 111 (2012) 053503.

[59] K.J.H. Mackay, N.A. Hill, Lattice Parameter and Hardness Measurements on High Purity Beryllium. J Nucl Mater 8 (1963) 263-264.

[60] R.L. Fleischer, R.J. Zabala, Mechanical properties of high-temperature beryllium intermetallic compounds. Metall Trans A 20 (1989) 1279-1282.

[61] M. Born, K. Huang. Dynamical theory of crystal lattices. Clarendon Press (1954) p. 142.

[62] F. Mouhat, F.X. Coudert. Necessary and sufficient elastic stability conditions in various crystal systems. Phys. Rev. B 90 (2014) 224104.

[63] M.G. Ganchenkova, V.A. Borodin, R.M. Nieminen, Hydrogen in beryllium: Solubility, transport, and trapping. Phys Rev B 79 (2009).

[64] M.G. Ganchenkova, P.V. Vladimirov, V.A. Borodin. Vacancies, interstitials and gas atoms in beryllium, J Nucl Mater 386-88 (2009) 79-81.

[65] Y. Fujii, M. Miyamoto, Jae-Hwan Kim, M. Nakamichi, N. Murayoshi, H. Iwakiri. Hydrogen retention behavior of beryllides as advanced neutron multipliers, Nucl Mater Energy 9 (2016) 233-236.

[66] M.G. Ganchenkova, V.A. Borodin, Ab initio study of small vacancy complexes in beryllium. Phys Rev B 75 (2007).

[67] M.L. Jackson, P.A. Burr, R.W. Grimes. Defect processes in Be12X (X = Ti, Mo, V, W), Nucl Fusion 57 (2017) 086049.

[68] H. Krimmel, M. Fähnle, Hydrogen and vacancies in the tokamak plasma-facing material beryllium. J Nucl Mater 255 (1998) 72-74.

[69] E. Hayward, B. Beeler, C. Deo, Multiple hydrogen trapping at monovacancies, Phil Mag Lett 92(5) (2012) 217-225.

[70] L. Sun, S. Jin, X.C. Li, Y. Zhang, G.H. Lu, Hydrogen behaviors in molybdenum and tungsten and a generic vacancy trapping mechanism for H bubble formation, J Nucl Mater 434 (2013) 395-401.

[71] Y.W. You, X.S. Kong, X.B. Wu, Y.C. Xu, Q.F. Fang, J.L. Chen, G.N. Luo, C.S. Liu, B.C. Pan, Z.G. Wang, Dissolving, trapping and detrapping mechanisms of hydrogen in bcc and fcc transition metals, Aip Adv 3(1) (2013).

[72] W.W. Xing, X.Q. Chen, Q. Xie, G. Lu, D.Z. Li, Y.Y. Li, Unified mechanism for hydrogen trapping at metal vacancies, Int J Hydrogen Energ 39(21) (2014) 11321-11327.

[73] S.M. Myers, P.M. Richards, W.R. Wampler, F. Besenbacher, Ion-Beam Studies of Hydrogen Metal Interactions, J Nucl Mater 165(1) (1989) 9-64.